Quenches and (pre)thermalization in a mixed Sachdev-Ye-Kitaev model

Ancel Larzul and Marco Schiró[*]

JEIP, USR 3573 CNRS, Collège de France, PSL Research University, 11, Place Marcelin Berthelot, 75231 Paris Cedex 05, France

We study the nonequilibrium quench dynamics of a mixed Sachdev-Ye-Kitaev model, with competing two-body random interactions leading to maximally chaotic non-Fermi liquid dynamics and a single body term which dominates at low temperatures and leads to Fermi liquid behavior. For different quench protocols, including sudden switching of two-body interaction and double quench protocols, we solve the large N real-time Dyson equation on the Keldysh contour and compute the dynamics of Green's functions from which we obtain effective temperature and relaxation rates. We show that the model thermalizes to a finite temperature equilibrium and that depending on the value of the quench parameters, the effective temperature can be below or above the Fermi-liquid to non-Fermi liquid crossover scale, which can then be accessed through the nonequilibrium dynamics. We identify quench protocols for which the heating dynamics slow down significantly—an effect that we interpret as a signature of prethermalization.

I. INTRODUCTION

Generic interacting quantum many-body systems are expected to thermalize when let to evolve unitarily under the action of their own Hamiltonian. The understanding of this quantum thermalization process, its possible slowdown or complete breakdown, is still a subject of large interest and effort in a broad community ranging from high-energy physics to condensed matter, atomic physics, and quantum information. A particularly interesting question concerns how fast a quantum many-body system can thermalize and therefore scramble the quantum information initially encoded in a quantum state.

The Sachdev-Ye-Kitaev model (SYK) [1–3], describing N Majorana fermions with random two-body all-to-all interactions, has played an important role in this context as a minimal model capturing thermalization, scrambling, and chaos [4–7] or analogously the emergence of strange metals in strongly interacting quantum matter [8,9].

Deformations of the SYK model have been actively discussed. An interesting example is the mixed SYK model, denoted in the following as the $SYK_4 + SYK_2$ model, where an additional random one-body all-to-all coupling (equivalent to a hopping term) is introduced. This model in thermal equilibrium has been shown to possess a crossover between a Fermi-liquid (FL) behavior and a non-Fermi-liquid (NFL) regime at low temperatures [10–12]. This feature, identified in related models of disordered quantum spins coupled to electrons [13–16] motivated by the physics of high-Tc superconductors, has recently attracted renewed experimental interest [17]. At finite N, this crossover in the mixed SYK model has been claimed to turn into a transition between

chaotic and integrable behavior [18–20], possibly related to many-body localization [21].

Much attention has been devoted to the low-energy equilibrium physics of these or related models, to their transport [22,23] or scrambling properties as encoded in the growth of out-of-time ordered correlators [24]. In particular, it was shown that the addition of a relevant perturbation at low energy makes the model less chaotic, with a Liapunov exponent vanishing as a quadratic power law in temperature [23,25–27]. In this respect, comparatively less work has focused on the genuine nonequilibrium dynamics of SYK models.

Dynamics in the pure SYK_4 model starting from different initial states, including completely uncorrelated ones as well as thermal states of the mixed SYK model, has been studied [28,29]. In the large N limit, it was shown that the system thermalizes to an equilibrium state at infinite temperature, unless the initial state is a correlated thermal state of the mixed $SYK_4 + SYK_2$ which leads to a finite effective temperature. More recent works have focused on the dynamics of mixed SYK models with complex fermions [30] or deformation of the SYK model possessing a quantum phase transition [31]. In the high-energy literature, the dynamics of pure states in the SYK model have attracted some interest [32], in particular, the dynamics of entanglement entropy [33]. Recently, the periodically driven mixed SYK has been investigated in Ref. [34].

In this paper, we study the nonequilibrium dynamics of the mixed $SYK_4 + SYK_2$ in the large N limit using Keldysh field theory techniques. Specifically, we solve the Kadanoff-Baym (KB) equations in real time and compare their solution with an approach based on a nonperturbative quantum Boltzmann equation (QBE). We start at initial time from the noninteracting SYK_2 model and consider different quench protocols, including a sudden switching of the two-body interactions and a double quench of the single-particle bandwidth and the interaction. We show that compared to the pure SYK_4, the dynamics shows a much richer thermalization landscape,

---
*On leave from Institut de Physique Théorique, Université Paris Saclay, CNRS, CEA, F-91191 Gif-sur-Yvette, France.

045105-1

including regimes of fast thermalization and of significant slowdown of heating that we interpret as prethermalization due to proximity to an integrable limit, the pure SYK_2 limit. Interestingly, we show that a simultaneous quench of single-particle bandwidth and interactions leads to a decrease of effective temperature and allows us to explore the crossover from NFL to FL through the quench dynamics and to obtain a nonequilibrium phase diagram for the problem.

The paper is structured as follows. In Sec. II, we introduce the model, the nonequilibrium protocol, and present the large-N KB equations for its real-time dynamics and discuss how to cast them in the form of a QBE. In Sec. III, we present our results for the sudden switching of random two-body interaction term, while in Sec. IV we consider the case of a double quench, in which both the interaction and the single-particle bandwidth are quenched with respect to the initial condition. Finally, in Sec. V we discuss our results in light of the thermodynamics of the mixed model and show that a double quench makes the effective temperature decrease and heating to slow down and identifies a signature of the crossover in the nonequilibrium decay rate evaluated at the effective temperature. In Sec. VI, we draw our conclusions, while Appendices A and B contain further technical details.

II. THE MIXED SYK MODEL

We study a generalization of the SYK model with both quartic and quadratic interactions [10–12] whose Hamiltonian reads

$$H(t) = \frac{i}{2} \sum_{i,j=1}^{N} J_{2,ij}(t) \chi_i \chi_j - \frac{1}{4!} \sum_{i,j,k,l=1}^{N} J_{4,ijkl}(t) \chi_i \chi_j \chi_k \chi_l, \tag{1}$$

where χ_i are Majorana fermions which satisfy $\{\chi_i, \chi_j\} = \delta_{ij}$. $J_{2,ij}(t)$ and $J_{4,ijkl}(t)$ are time-dependent random independent Gaussian variables with zero mean and variances $\overline{J_{2,ij}^2(t)} = \frac{J_2^2(t)}{N}$ and $\overline{J_{4,ijkl}^2(t)} = \frac{3! J_4^2(t)}{N^3}$.

As we will discuss more in detail in Sec. III, we consider as an initial condition the ground state of the pure SYK_2 model and the quench protocol $J_2(t) = \theta(-t)J_{2,i} + \theta(t)J_{2,f}$ and $J_4(t) = \theta(t)J_4$, leaving the possibility to have $J_{2,i} = J_{2,f}$. In this way, we can study both the effect of a pure quench of J_4 as well as the combined effect of switching on the interaction and changing the bandwidth of the Majorana fermions.

At equilibrium and in the large N limit, the SYK model with zero hopping $J_2 = 0$ describes a NFL where the single-particle Green's function in imaginary time decays as $G(\tau) \sim 1/\sqrt{\tau}$. However, this phase is not stable to the introduction of the hopping term $J_2 \neq 0$, which constitutes a relevant perturbation and the system turns into a FL with single-particle Green's function $G(\tau) \sim 1/\tau$. A crossover between the FL and NFL is expected to happen when the hopping term becomes dominant which corresponds to an energy (or temperature) scale $T^* \sim J_2^2/J_4$ [13,22]. As we mentioned in the Introduction, the situation is even more interesting at finite N where the crossover turns into a transition between chaotic and integrable regimes. Here we will not consider the finite N case and focus on the thermodynamic limit and the resulting

real-time dynamics that can also be solved exactly through saddle-point techniques as we briefly discuss below.

A. Large-N real-time Dyson equation

The real-time dynamics of the mixed SYK model can be obtained in the large-N limit through saddle-point methods on the Keldysh action [28,35]. In particular, the real-time Green's function of the Majorana fermions, defined as

$$G^{\alpha\beta}(t_1, t_2) = -\frac{i}{N} \sum_i \langle \chi_i^\alpha(t_1) \chi_i^\beta(t_2) \rangle, \tag{2}$$

with $\alpha, \beta = \pm$ Keldysh contour index, can be shown to satisfy a real-time Dyson equation of the form

$$[\hat{G}_0^{-1} - \hat{\Sigma}] \circ \hat{G} = 1, \tag{3}$$

where $[\hat{G}_0^{-1}]^{\alpha\beta}(t_1, t_2) = i\alpha \delta_{\alpha\beta} \delta(t_1 - t_2) \partial_{t_1}$ is the free Majorana fermion Green's function, the self-energy reads

$$\Sigma^{\alpha\beta}(t_1, t_2) = -\alpha\beta J_4(t_1) J_4(t_2) G^{\alpha\beta}(t_1, t_2)^3 + J_2(t_1) J_2(t_2) G^{\alpha\beta}(t_1, t_2), \tag{4}$$

and the symbol $\circ$ denotes real-time convolution. For Majorana fermions, it is convenient to work with the greater (lesser) Green's function $G^{>(<)}(t_1, t_2)$, which are related as

$$G^>(t_1, t_2) = -G^<(t_2, t_1), \tag{5}$$

and from which one can obtain all the relevant Green's functions:

$$G^R(t_1, t_2) \equiv \theta(t_1 - t_2)(G^>(t_1, t_2) - G^<(t_1, t_2)), \tag{6}$$

$$G^A(t_1, t_2) \equiv -\theta(t_2 - t_1)(G^>(t_1, t_2) - G^<(t_1, t_2)), \tag{7}$$

$$G^K(t_1, t_2) \equiv G^>(t_1, t_2) + G^<(t_1, t_2). \tag{8}$$

The first Schwinger-Dyson equation can be put into a more convenient form known as the KB equations [36]:

$$i\partial_{t_1} G^{>,<}(t_1, t_2) = \int_{-\infty}^{+\infty} dt \, \Sigma^R(t_1, t) G^{>,<}(t, t_2) + \int_{-\infty}^{+\infty} dt \, \Sigma^{>,<}(t_1, t) G^A(t, t_2), \tag{9}$$

$$-i\partial_{t_2} G^{>,<}(t_1, t_2) = \int_{-\infty}^{+\infty} dt \, G^R(t_1, t) \Sigma^{>,<}(t, t_2) + G^{>,<}(t_1, t) \Sigma^A(t, t_2). \tag{10}$$

Likewise, we define the retarded and advanced self-energies:

$$\Sigma^R(t_1, t_2) \equiv \theta(t_1 - t_2)(\Sigma^>(t_1, t_2) - \Sigma^<(t_1, t_2)), \tag{11}$$

$$\Sigma^A(t_1, t_2) \equiv -\theta(t_2 - t_1)(\Sigma^>(t_1, t_2) - \Sigma^<(t_1, t_2)). \tag{12}$$

We mention here for future use that the greater Green's function of the pure SYK_2 model ($J_2(t) = J_2$, $J_4(t) = 0$) is known exactly, at least in the long-time stationary limit (i.e., time-translational-invariant limit),

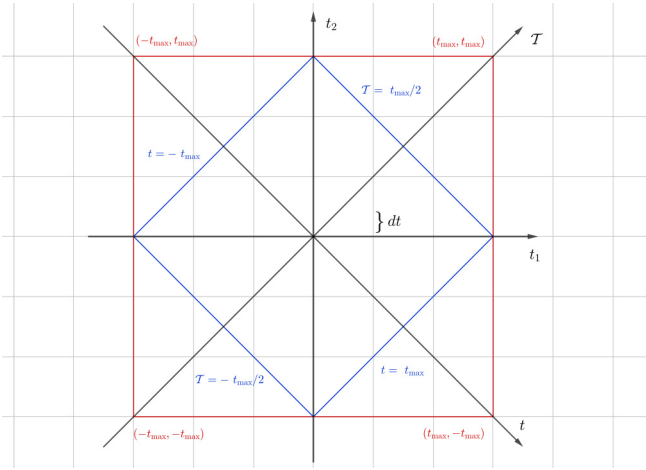$$G_2^>(t) = \frac{-i}{2J_2 t}(J_1[2J_2 t] - iH_1[2J_2 t]), \tag{13}$$

FIG. 1. Sketch of the t_1, t_2 plane as well as the rotated plane $\mathcal{T}, t$.

where $J_1(x)$, $H_1(x)$ are special (Bessel's and Henkel's) functions of the first kind.

1. Numerical integration of Kadanoff-Baym equations

In this paper, we solve the KB Eqs. (9) and (10) numerically on a $t_1 - t_2$ grid of size 2001×2001, 4001×4001, or 6001×6001 with time step $dt = 0.05$. The grid has a length $2 t_{max}$ in each direction as shown in red in Fig. 1. Initially, at times $t_1, t_2 < 0$ the system is prepared in the ground state of the pure SYK_2 model with coupling $J_2 = 0.5$. We solve KB equations for $G^>$ on the grid by using a predictor-corrector scheme [28,29,31]. Integrals are computed using the trapezoidal rule. We verify the consistency of our numerical code by checking the conservation of energy and the normalization of the spectral density. Thermal equilibrium solutions for a given inverse temperature β are obtained by solving the Schwinger-Dyson equation self-consistently following Ref. [28]' further details are discussed in Appendix A.

B. Observable of interest: Spectral and distribution functions

To interpret the results obtained by the numerical integration of the real-time KB equations, it is convenient to introduce a mixed time-frequency representation for the Green's functions defined in the previous section. Specifically, we can change the time coordinates (t_1, t_2) to an average and relative time coordinates $(\mathcal{T}, t)$ defined as

$$\mathcal{T} = \frac{t_1 + t_2}{2}, \quad t = t_1 - t_2. \tag{14}$$

The bounds of the $(\mathcal{T}, t)$ grid are shown in blue in Fig. 1. Notice that on this grid the initial conditions corresponds to $\mathcal{T} = -\mathcal{T}_{max}$ and the maximum $\mathcal{T}$ value to $\mathcal{T} = \mathcal{T}_{max}$ with $\mathcal{T}_{max} = t_{max}/2$.

Taking the Fourier transform with respect to the relative time t, we define the so-called Wigner transform of the Green's functions [28,35]:

$$G(\mathcal{T}, \omega) = \int dt\, e^{i\omega t} G\left(t_1 = \mathcal{T} + \frac{t}{2}, t_2 = \mathcal{T} - \frac{t}{2}\right). \tag{15}$$

This has the advantage of explicitly showing the effect of time-translation symmetry breaking due to the quench and

resulting in an explicit dependence on the average time $\mathcal{T}$. Furthermore, it suggests a picture of slow-varying quasiequilibrium which connects naturally with the long-time limit in which one expects the approach to thermal equilibrium.

Using the Wigner transform, we can define quantities which have a direct physical interpretation such as the time-dependent spectral function $A(\mathcal{T}, \omega)$,

$$A(\mathcal{T}, \omega) = -2\mathrm{Im}G^R(\mathcal{T}, \omega), \tag{16}$$

or distribution function $F(\mathcal{T}, \omega)$,

$$iG^K(\mathcal{T}, \omega) = F(\mathcal{T}, \omega)A(\mathcal{T}, \omega), \tag{17}$$

using a parametrization of the Keldysh Green's function which explicitly evokes a fluctuation-dissipation theorem. In fact, in thermal equilibrium, corresponding to the initial condition or possibly the long-time behavior if thermalization is established, those two quantities are time independent and related by a universal identity, the fluctuation-dissipation theorem [37],

$$iG^K(\omega) = \tanh\left(\frac{\beta\omega}{2}\right)A(\omega), \tag{18}$$

where β is the inverse temperature.

C. Quantum Boltzmann equation approach

In this section, we discuss a different way of solving the KB Eqs. (9) and (10), which is based on a coarse-grained approach in the time domain, focusing on the long-time dynamics rather than on the short-time transient. This idea can be formalized by performing a Wigner transform of the KB equations followed by a gradient expansion in the *slow* average time $\mathcal{T}$, which casts the KB equation into a quantum kinetic (Boltzmann) equation [35] for the Wigner-transformed distribution $F(\mathcal{T}, \omega)$. Performing these steps for our mixed SYK model, we obtain (as we discuss in detail in Appendix B), to the lowest order in the gradient expansion, the equation

$$\partial_{\mathcal{T}} F(\mathcal{T}, \omega) = I^{\mathrm{coll}}[F(\mathcal{T}, \omega)], \tag{19}$$

where the collision integral I^{coll} reads

$$\begin{aligned} I^{\mathrm{coll}}[F(\mathcal{T}, \omega)] = {}&i\Sigma^K(\mathcal{T}, \omega) - iF(\mathcal{T}, \omega) \\ &\times (\Sigma^R(\mathcal{T}, \omega) - \Sigma^A(\mathcal{T}, \omega)), \end{aligned} \tag{20}$$

and we emphasize that the self-energy components $\Sigma^R(\mathcal{T}, \omega)$, $\Sigma^A(\mathcal{T}, \omega)$, and $\Sigma^K(\mathcal{T}, \omega)$, which can be obtained from Eq. (4) after Wigner transform, also depend on the distribution function itself (see Appendix B for their explicit expression). The dynamics of the distribution function $F(\mathcal{T}, \omega)$ is in principle coupled, through the full KB equations, to the dynamics of the spectral function $A(\mathcal{T}, \omega)$ which also enters the self-energies in Eq. (20). However, to the lowest order in the gradient expansion, one can show that the dynamics of the spectral function is simply given by

$$\partial_{\mathcal{T}} A(\mathcal{T}, \omega) = 0, \tag{21}$$

i.e., the spectral function of the system is already stationary while the distribution function is still slowly evolving. As we are going to see in the next section, this separation of
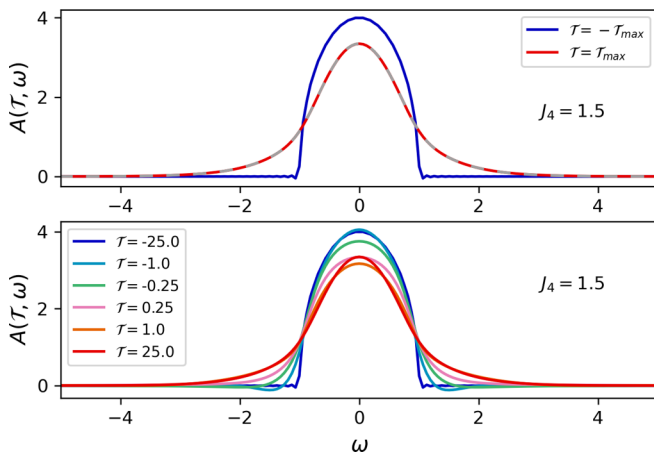
FIG. 2. Transient spectral function after a sudden switch-on of J_4 in the mixed SYK model. Top: Spectral function at initial time ($\mathcal{T} = -\mathcal{T}_{\max}$) and at long times ($\mathcal{T} = \mathcal{T}_{\max}$), compared to the equilibrium spectral function of the mixed $SYK_4 + SYK_2$ model at the final temperature (dashed grey line), confirming thermalization and evolution of the spectral function for different times $\mathcal{T}$.

timescales between spectrum and occupation is to a good extent present in the full solution of the KB equations, thus supporting the validity of the lowest order gradient expansion, at least for what concerns the long-time dynamics. Before closing, it is worth emphasizing that, traditionally, QBE approaches have been used together with perturbative evaluations of the collision integral and under specific assumptions on the spectral properties of the systems (quasiparticle approximation). Here, instead, our collision integral in Eq. (20) is *exact* due to the large-N nature of the SYK problem. We note that, recently, similar QBE approaches have been developed to describe the real-time dynamics of other strongly interacting quantum many-body systems beyond perturbation theory [38–40].

III. RESULTS: QUENCH OF J_4

In this section, we present our results for the dynamics of the mixed SYK model as obtained from the solution of the real-time Dyson equation. Specifically, we first consider a sudden switching of the quartic interaction $J_4(t) = \theta(t)J_4$, starting from a pure SYK_2 model in its ground state and with $J_2 = 0.5$. Later, in Sec. IV we will consider the effect of quenching both J_2 and J_4.

A. Transient spectral function and thermalization of the mixed SYK model

We start discussing the evolution of the spectral function $A(\mathcal{T}, \omega)$ after a quench to $J_4 = 1.5$. In Fig. 2, we plot the initial spectral function of the SYK_2 model, which features the well-known sharp edge semicircular density of state, and its long-time limit after the switching on of the J_4 interaction, featuring a much broader resonance with tails at higher frequencies. We compare the latter with the equilibrium spectral function of the mixed SYK model evaluated at the final temperature (see next section) and find a perfect match, thus confirming that the mixed SYK model reaches thermal equi-
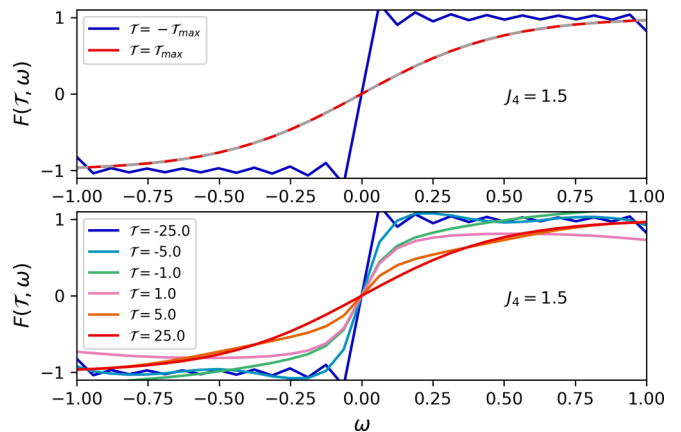

FIG. 3. Transient distribution function after a sudden switch-on of J_4 in the mixed SYK model. Top: Distribution function at initial and final times and its dynamical evolution showing the onset of heating (finite temperature). Parameters: $J_2 = 0.5$, $J_4 = 1.5$.

librium. In the bottom panel, we plot the evolution of the spectral function $A(\mathcal{T}, \omega)$ as a function of increasing time $\mathcal{T}$. We see that spectral features at high frequencies reshape rather rapidly after the quench, with tails forming above the bandwidth set by J_2, while the low-frequency features follow at later times.

B. Distribution function and dynamics of effective temperature

A further demonstration of the onset of thermalization in the mixed SYK model comes from the dynamics of the distribution function, $F(\mathcal{T}, \omega)$, defined in Eq. (17), that we plot in Fig. 3. As previously, we show in the top panel the initial condition and the long-time limit, while in the bottom panel the evolution of the distribution function for different average times $\mathcal{T}$. As the initial state is taken at zero temperature, the distribution function is rather sharp around low frequency, while a long time after the quench, a smoother behavior is approached, indicating the development of a higher final temperature. From the bottom panel, we can see that, as for the spectral function, the high-frequency features of the distribution are those that readjust faster after the quench, while the low-frequency sector takes a longer time to respond. Furthermore, by comparing Figs. 2 and 3, one can conclude that the dynamics of the spectral function is typically faster than the one of the distribution function.

To better understand the onset of thermalization, we note that throughout the evolution the low-frequency behavior of the distribution function is linear in frequency, which suggests extracting a time-dependent effective temperature $T_{\text{eff}}(\mathcal{T})$ by fitting the low-frequency behavior of $F(\mathcal{T}, \omega)$ with $\tanh(\beta_{\text{eff}}(\mathcal{T})\omega/2)$. We plot the dynamics of this effective temperature for different values of J_4 in Fig. 4. We see that for small quenches, the system remains close to the ground state and the effective temperature changes slowly with time. One can understand this slowing down of heating in the weak quench regime in terms of a prethermalization phenomenon [41–43] found in other quench problems of interacting quantum many-body systems and associated to the proximity to an integrable point—in the present case, the pure SYK_2 model.
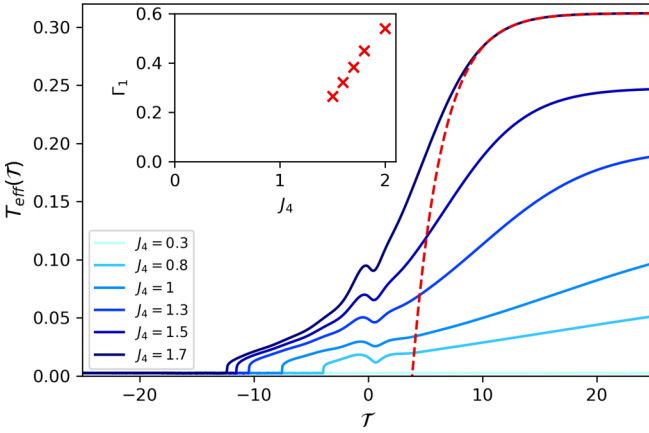
FIG. 4. Dynamics of the effective temperature $T_{\mathrm{eff}}(\mathcal{T})$, extracted from the distribution function as discussed in the main text, for different values of the J_4 interaction. We see that the heating dynamics of the system strongly depends on the value of J_4.

On the other hand, increasing the strength of the quench J_4 leads to a faster heating dynamics. The approach to the long-time limit, that we identify with the final temperature reached by the system after the quench, $T_f = T_{\mathrm{eff}}(\infty)$, is exponential,

$$T_{\mathrm{eff}}(\mathcal{T}) - T_f = A \exp\left(-\Gamma_1 \mathcal{T}\right),$$

from which we can extract a thermalization rate Γ_1 that depends, in general, on the quench parameters, in particular, on the final value of J_4, as we show in the inset. In particular, for quenches of intermediate strength, we find $\Gamma_1 \sim J_4$, while upon decreasing we expect a subleading behavior, possibly quadratic in J_4. However, the timescales needed to reach equilibrium exceed our $\mathcal{T}_{\max}$, therefore we cannot conclude the nature of this scaling (see, however, next section).

C. Comparison with QBE approach

We now compare the dynamics obtained from the full solution of the KB equations with the QBE approach discussed in Sec. II C. To this extent, we focus on a sudden switching of the J_4 interaction, keeping the J_2 coupling fixed. An important issue when performing this comparison concerns the choice of initial conditions for the distribution and spectral function entering the QBE approach. As we have seen, the spectral function remains constant in time at the lowest order approximation [see Eq. (21)], thus we take it to be equal to the equilibrium spectral function of the final Hamiltonian at the final effective temperature. The idea behind this choice is that, as the full KB solution shows, the spectral function thermalizes on much faster timescales than the distribution function. For what concerns the distribution function, the issue is more subtle since any equilibrium thermal-like distribution annihilates the collision integral, independently of the value of the temperature (see Appendix B). We therefore choose to take as our initial condition the distribution function obtained by solving the full KB equations for a short-time interval $\mathcal{T}_0 = 5$. In Fig. 5, we plot, for the quench $(J_{2,i} = 0.5, 0) \rightarrow (J_{2,f} = J_{2,i}, J_4 = 1.5)$, the evolution in time of the QBE distribution function from the initial $\mathcal{T} = \mathcal{T}_0 = 5$ to late times, and show that it correctly relaxes to the thermally equilibrated
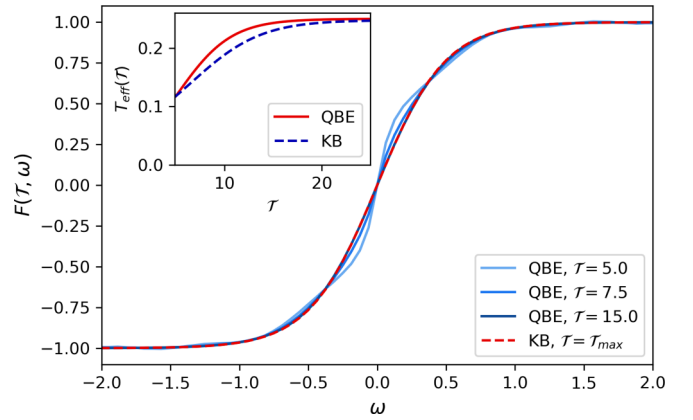

FIG. 5. Evolution of the distribution function $F(\mathcal{T}, \omega)$ at different times compared with the long-time limit obtained from the full solution of the KB equations. Inset: Evolution of the time-dependent effective temperature obtained by fitting the QBE distribution function at low frequency, compared with the one obtained from KB equations. Quench parameters: $(J_{2,i} = 0.5, 0) \rightarrow (J_{2,f} = J_{2,i}, J_4 = 1.5)$.

one (red-dashed lines) obtained from the KB dynamics. In the inset, we compare the dynamics of the effective temperature extracted with the two methods. We confirm that the discrepancy between QBE and KB dynamics is mainly in the intermediate transient while the long-time asymptotics is well captured.

D. Real-time retarded Green's functions: Long-time decay rate and waiting time dependence

We now discuss the dynamics of the retarded Green's function in the time domain, focusing, in particular, on its long time decay. From the analysis of the spectral function presented in the previous section, it appeared difficult to discuss the effect of the quench on the low-frequency behavior of the spectrum, a feature that will appear more clearly in the time domain. In the left panel of Fig. 6, we plot the retarded Green's function $G^R(\mathcal{T}, t)$ a long time after the quench, i.e., for $\mathcal{T} = \mathcal{T}_{\max}$, as a function of the relative time t and for different values of J_4.

We first note that the Green's function shows pronounced oscillations, with a period which appears to be independent of J_4 and completely set by the J_2 scale. This can be understood by considering the analytic expression for the Green's function of the pure SYK_2 model given in Eq. (13), which indeed shows oscillations with a frequency set by J_2.

Concerning the long-time decay, we see that with the exception of the very small quench regime, where the Green's function remains closer to the one of a pure SYK_2 which decays as a power law, the system rapidly enters into an exponential decay regime as a function of the relative time, which is compatible with the Lorentzian line shape found in the frequency-resolved spectral function (see Fig. 2). We can therefore extract a decay rate for the stationary retarded Green's function using an ansatz of the form

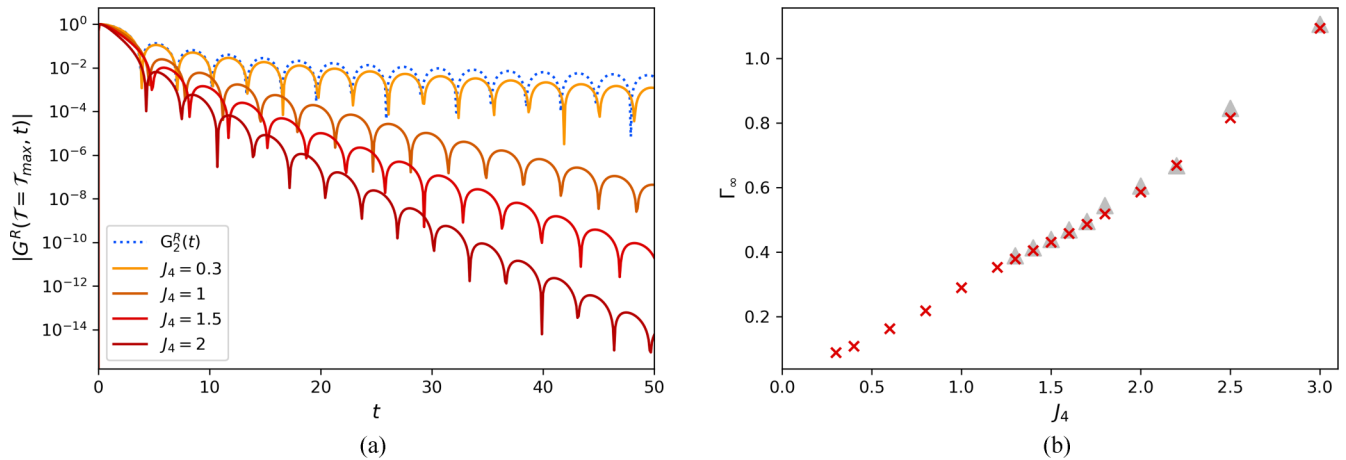$$G^R(\mathcal{T}_{\max}, t) \sim \exp(-\Gamma_\infty t). \tag{22}$$

(a)

(b)

FIG. 6. (a) Real-time retarded Green's function as a function of the relative time t long after the quench ($\mathcal{T} = 25$) for different J_4. We compare the decay with the power-law behavior expected for a pure SYK_2 (dotted blue line). (b) Exponential decay rate Γ_∞ extracted from the large $\mathcal{T}$ limit of the retarded Green's function for different J_4 (red crosses). The grey triangles are the decay rates extracted from the equilibrium Green's function at T_f.

As for the thermalization time discussed before, the decay rate Γ_∞ depends, in general, on the quench parameters—in particular, the value of the interaction J_4, as we plot in the right panel of Fig. 6, is very small for $J_4 \to 0$, reflecting the power-law decay of the pure SYK_2 model, and grows upon increasing the strength of the quench, showing a linear behavior at intermediate couplings and a superlinear regime for large J_4. Finally, we expect (not shown) the decay rate to saturate at larger values of J_4.

We now move on to discuss the waiting time dependence of the real-time retarded Green's function, which further allows us to clarify how the initial power-law decay regime and the long-time exponential decay regime are connected as the average time $\mathcal{T}$ is increased. In Fig. 7, we plot the
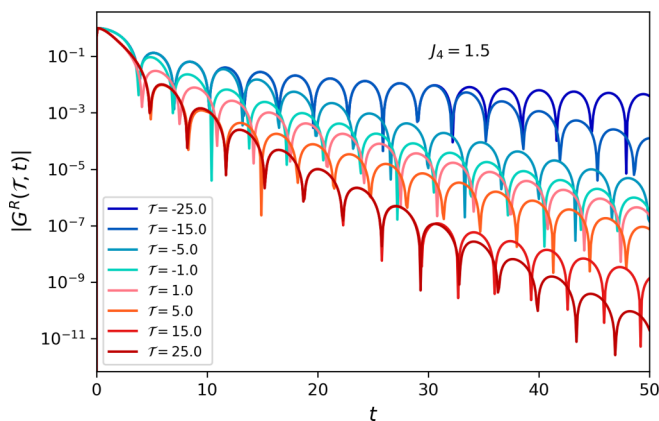

FIG. 7. Waiting time dependence of the real-time retarded Green's function after a quench of $J_4 = 1.5$. At short average times, the decay as a function of the relative time t is power law, reflecting the initial low-temperature state of the SYK_2 model. Upon increasing the time after the quench $\mathcal{T}$, the decay crosses over to an exponential decay, around a time $t \sim 2\mathcal{T}$. We note that the decay at long times is exponential, yet with a decay rate which is slower than the long-time limit Γ_∞. This behavior is compatible with an ansatz of the form 23 for the two-time Green's function.

real-time retarded Green's function, $G^R(\mathcal{T}, t)$, as a function of the relative time, for different average times $\mathcal{T}$ and for a quench to $J_4 = 1.5$. We recognize a characteristic feature of this two-time Green's function, namely, a short-time behavior and long-time regimes with a crossover at times $t \sim 2\mathcal{T}$. We also notice that the short-time behavior is a power law for negative average times $\mathcal{T} < 0$, corresponding to the regime of influence of the initial condition, while it is exponential for positive average times $\mathcal{T} > 0$. The numerical results suggest an ansatz of the form

$$G^R(\mathcal{T}, t) = G^R_\infty(t) f(\mathcal{T}, t), \qquad (23)$$

where $f(\mathcal{T}, t)$ is a function chosen to capture the crossover and the short-/long-time behavior of the two-time retarded Green's function [44]. In particular, for positive times $\mathcal{T} > 0$, we have that $f \simeq 1$ for $t \ll 2\mathcal{T}$ while it grows exponentially for long times, i.e., $f \sim \exp(\Gamma' t)$ for $t \gg 2\mathcal{T}$, with a rate Γ' which is, in general, smaller than the long-time asymptotic rate Γ_∞, leading to a slow down of the decay rate at finite positive waiting times, as shown in Fig. 7.

IV. RESULTS: QUENCH OF J_4 AND J_2

The results of the previous section have shown that under a sudden switching of the interaction, the mixed SYK model thermalizes rapidly, with a significant increase of the effective temperature, except for weak quenches $J_4 \ll J_2$ where a much slower heating dynamics is observed that we have interpreted as a signature of prethermalization. To explore further the thermalization pathways of the mixed SYK model and to connect them to its equilibrium properties, in particular, to the NFL to FL crossover, in this section we consider a double quench protocol where in addition to the sudden switching of the J_4 interaction, the system at time $t = 0$ also undergoes a quench of the single-particle term $J_{2,i} = 0.5 \to J_{2,f} \neq J_{2,i}$. Protocols of this sort have been discussed before in the literature on quantum quenches; see, for example, Refs. [44–46] with the idea of disentangling the role of integrability-breaking and generic nonequilibrium
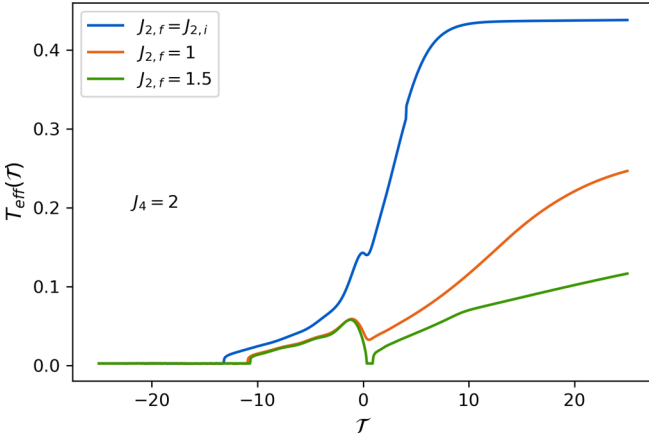
FIG. 8. Dynamics of the effective temperature $T_{\text{eff}}(\mathcal{T})$ after a double quench of J_2 and J_4. We consider a sudden switching-on of J_4 from zero to $J_4 = 2$ and different quench values of $J_{2,f}$. We see that the heating dynamics of the system slows down upon increasing the strength of the J_2 quench, a sign of extended prethermalization dynamics.
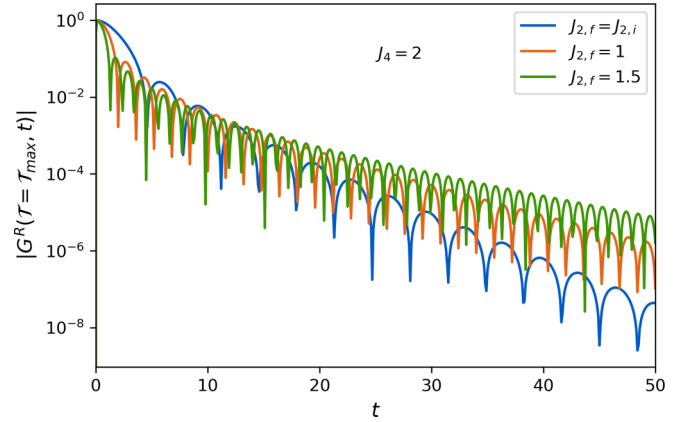

FIG. 9. Decay of real-time retarded Green's function $G^R(\mathcal{T}, t)$, long after the quench, as a function of the relative time t after a double quench of J_2 and J_4. We consider a sudden switching-on of J_4 from zero to $J_4 = 2$ and different quench values of $J_{2,f}$. We see that the decay rate is slower upon increasing the quench of J_2.

perturbations in the heating production and thermalization pathways of quantum systems. We emphasize that while the equilibrium properties of the mixed SYK model are completely controlled by the adimensional ratio J_4/J_2, for the nonequilibrium dynamics, there are, in principle, two independent adimensional quantities, $J_{2,f}/J_{2,i}$ and $J_4/J_{2,f}$, the former controlling the degree of excitation of single-particle states while the latter the role of interactions. One can naively expect that when single-particle excitations dominate over interactions, scattering processes are kinematically blocked, resulting in a slow down of heating. As we are going to show below, this double quench protocol indeed provides us with an additional tuning parameter to explore the low-heating regime of the mixed SYK quench dynamics.

A. Dynamics of effective temperature and real-time decay of retarded Green's function

To discuss the effect of this double quench, we focus on the dynamics of the effective temperature as obtained from the low-frequency regime of the distribution function as discussed in Sec. III. In particular, we plot in Fig. 8 the effective temperature for a quench to $J_4 = 2$ and different values of the $J_{2,f}$ parameter. We see that quenching the J_2 term leads to a significant slowdown of the effective temperature dynamics as compared to the case in which J_2 is kept constant (top line in Fig. 8), and already for $J_{2,f} = 1.5$ the effective temperature does not reach a stationary state on the timescales of our simulation. In addition to a slowing down of the thermalization time, we also note that the long-time limit of the effective temperature is reduced by the quench, namely, the system heats up less.

This can be understood by noticing that, at least for $J_{2,f} \gg J_4$ when the interactions can be neglected to a leading order, the final and initial Hamiltonian are both solvable SYK_2 models, a regime in which the dynamics is known to equilibrate instantaneously without heating production.

The slowdown of the dynamics in the presence of a J_2 quench can also be clearly seen from the decay in time of the retarded Green's function a long time after the quench, as discussed for a single quench in Sec. III. In Fig. 9, we plot $G^R(\mathcal{T}, t)$ a long time after the quench $\mathcal{T} = 25$ as a function of the relative time t, after a quench to $J_4 = 2$ and different values of the J_2 quench. We see that the decay is always exponential, as in the case of a single quench discussed in Eq. (22) although with a rate Γ_∞ (not shown), which decreases upon increasing $J_{2,f}/J_{2,i}$.

V. DISCUSSION: QUENCH-INDUCED NFL TO FL CROSSOVER

We now summarize our results for the quench dynamics of the mixed $SYK_4 + SYK_2$ model. Our analysis so far has focused on the dependence of the nonequilibrium dynamics from the quench parameters, respectively, the strength of the interaction J_4 and of the single-particle quench $J_{2,f}/J_{2,i}$. An interesting question we would like to address here is how the long-time limit of the quench problem relates to the equilibrium properties of the mixed SYK model and whether, in particular, it is possible to explore the crossover from NFL to FL in the quench dynamics.

To this extent, it is useful to plot a dynamical phase diagram for the quench problem, as in Fig. 10, where we show the dependence of the effective temperature T_f from the quench parameter J_4 for different values of the J_2 quench, corresponding, respectively, to a single quench ($J_{2i} = J_{2f}$) and to a double quench ($J_{2i} \neq J_{2f}$). The effective temperature is obtained from the dynamics of the distribution function (points in Fig. 10), as discussed in Sec. III, and further compared to the estimate obtained from total energy conservation (lines in Fig. 10, as discussed in Appendix A). We see that T_f increases with J_4, namely, the stronger the value of the interaction quench the more the system heats up, however, this increase is slower for a double quench protocol. Specifically, we see that upon increasing the single-particle coupling term $J_{2f}/J_{2i} > 1$, at
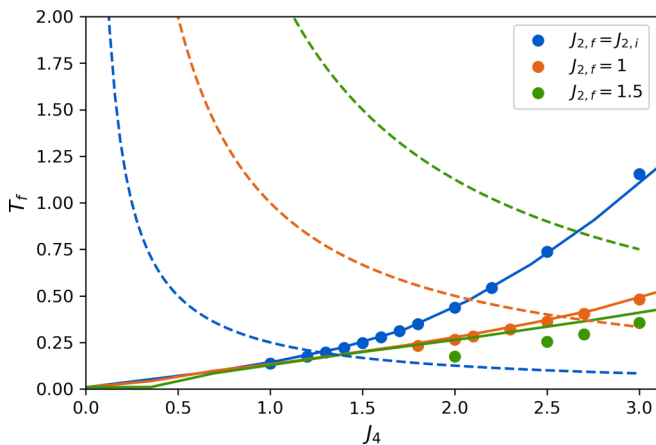
FIG. 10. Quench phase diagram for the mixed SYK$_4$ + SYK$_2$ model. Effective final temperature versus the quench parameter J_4 and for different quenches of the J_2 term. We see that quite generically the effective temperature production is slower upon also quenching J_2. For comparison, we plot in the same plane the crossover scale $T^* \sim J_{2,i}^2/J_4$ and $T^* \sim J_{2,f}^2/J_4$, corresponding to the equilibrium FL-to-NFL crossover.

FIG. 11. Out-of-equilibrium scattering rate, defined as the imaginary part of the retarded self-energy long time after the quench, $-\operatorname{Im}\Sigma^R(\mathcal{T} = \mathcal{T}_{\max}, \omega = 0)$, as a function J_4 for a single quench (blue points) or for a double quench to $J_{2,f} \neq J_{2,i}$ (orange and green points). Grey triangles: Equilibrium result at T_f. Inset: Same quantity plotted versus the effective temperature T_f, showing a linear scaling and deviations from it at lower effective temperatures.

fixed $J_4/J_{2,i}$ ratio, the final temperature at which the system effectively thermalizes is lower as compared to a pure J_4 quench. This can be easily understood in the regime $J_4 \ll J_{2,i}$, when essentially the dynamics reduces to a quench between SYK$_2$ models which are known not to produce substantial heating, but remains true even at intermediate values of J_4 as our numerical results show. This result indicates that the out-of-equilibrium physics of the mixed SYK model is much richer than the pure SYK$_4$ and that changing the quench protocol allows us to explore different dynamical regimes. This result is particularly interesting in connection with the scale $T^* \sim J_{2,f}^2/J_4$ that controls the equilibrium properties of the final mixed SYK model and, in particular, its NFL-to-FL crossover. For comparison, we plot these energy scales on the same plane as the effective final temperature, see Fig. 10. For a single quench of the interaction term J_4, we see that most of our data lie above the crossover scale and therefore we expect to see a behavior compatible with a pure SYK$_4$. On the other hand, for a double quench the effective temperature decreases and the crossover line is also pushed to larger values of J_4. As a result, quenching the single-particle scale, we expect to see a behavior which is more compatible with a pure SYK$_2$. To confirm this expectation, we consider the out-of-equilibrium scattering rate for the Majorana fermions, namely, the imaginary part of the retarded self-energy long time after the quench, $-\operatorname{Im}\Sigma^R(\mathcal{T} = \mathcal{T}_{\max}, \omega = 0)$. This can be readily obtained from the nonequilibrium Green's functions through Eqs. (11) and (4) and after Wigner transform. In thermal equilibrium, this quantity is known to be sensitive to the crossover scale T^*, as we discuss in Appendix A. In Fig. 11, we plot this quantity as a function of J_4 for different values of $J_{2,f}$ and $J_{2,i}$, therefore including both the single quench protocol discussed in Sec. III as well as the double quench. As expected, the scattering rate, much like the effective temperature, increases with J_4 but with a rate that depends strongly on $J_{2,f}/J_{2,i}$ and decreases for large quenches of the J_2 coupling. To further
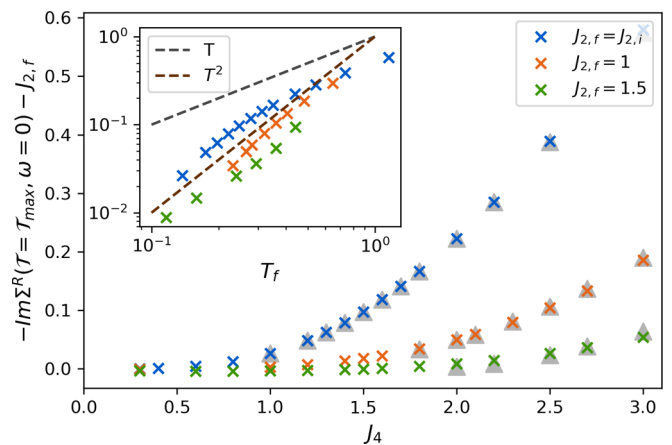
confirm the overall thermalization of the nonequilibrium dynamics, we compare this quantity with its equilibrium version at the final effective temperature (see grey triangles), finding perfect agreement. Furthermore, in the inset of Fig. 11 we plot the same scattering rate as a function of the effective temperature T_f for the three values of $J_{2,f}/J_{2,i}$ considered. We see that for a double quench when the effective temperature decreases while the crossover scale is pushed towards higher values, we are able to see more clearly a behavior which is consistent with the FL scaling

$$-\operatorname{Im}\Sigma^R \sim T_f^2, \tag{24}$$

On the other hand for a single quench, corresponding to $J_{2,f} = J_{2,i}$, when the effective temperature is above the crossover scale (See Fig. 9) the scattering rate deviates from the FL scaling of Eq. (24) and is compatible with the behavior expected from SYK$_4$ at intermediate temperatures (see Appendix A), when the square-root low temperature regime crosses over to a linear scaling. We emphasize that reaching lower effective temperatures in our dynamical approach is challenging since the dynamics slow down significantly and the long-time stationary limit becomes inaccessible to our finite time simulation. Nevertheless, based on the evidence in Fig. 11 we can safely conclude that the scattering rate is a good probe of the quench-induced crossover between NFL and FL. In conclusion, we note that, on the other hand, the relaxation rate Γ_∞ defined from the long-time limit of the retarded Green's function is not a good probe of the crossover already in equilibrium, as we show explicitly in Appendix A. An interesting point that we leave for future work is whether one can draw a formal connection between probes of thermalization and chaos obtained through the Lyapunov exponent of out-of-time ordered correlators and the scattering rate obtained through single-particle self-energies and Green's functions.

VI. CONCLUSIONS

In this paper, we have discussed the quench dynamics of the mixed $SYK_4 + SYK_2$ model in the large N limit. Specifically we have solved the real-time KB equations numerically for two different quench protocols, corresponding to a sudden switching of the J_4 interaction and a simultaneous quench of the single-particle bandwidth J_2. We have compared the full KB dynamics to an approach based on a QBE, derived starting from the exact large N Dyson equation without any quasiparticle approximation. We have shown that this approach, which relies on a gradient expansion for a slow average time, is able to capture correctly the long-time dynamics of the problem.

Our results have shown that quite generically the unitary dynamics of this model thermalizes to a finite temperature thermal equilibrium state, as confirmed by both the spectral function and the distribution functions of the Majorana modes, two quantities that, however, evolve on much different timescales. In particular, the dynamics of the effective temperature as obtained from the effective Fluctuation-Dissipation Theorem (FDT) on the distribution function appears to become very slow for weak quenches or, equivalently, for large quenches of the single-particle term J_2. We have connected this result to the onset of prethermalization in the quench dynamics of this system.

As compared to quenches in the pure SYK_4 model, the mixed case enjoys a much richer dependence from the quench parameters, encapsulated in the nonequilibrium phase diagram shown in Fig. 10. We have shown that, quite generically, a quench of the J_4 coupling leads to a finite temperature which can be above or below the crossover scale T^* and that quenching the single-particle term J_2 significantly reduces the heating in the system and allows us to access the NFL to FL crossover through the quench dynamics, as we have shown by looking at the nonequilibrium scattering rate at long times.

Our results therefore offer a complementary picture, based on the full out-of-equilibrium dynamics, to the studies on the scrambling properties of the mixed SYK model and point out a possible interesting connection between slow scrambling and prethermalization that could be worth discussing further in the future. Further perspectives opened by this work include the investigation of different nonequilibrium settings involving mixed SYK-like models, such as those recently considered in connection with traversable wormholes in the high-energy literature. Finally, we note that there is currently large interest in disordered fully connected models with mixed competing interactions which, even at the classical level, have been shown to possess intriguing properties [47].

APPENDIX A: EQUILIBRIUM PROPERTIES OF THE MIXED SYK MODEL

In this Appendix, we briefly recall some of the equilibrium properties of the mixed $SYK_4 + SYK_2$ model in the large N
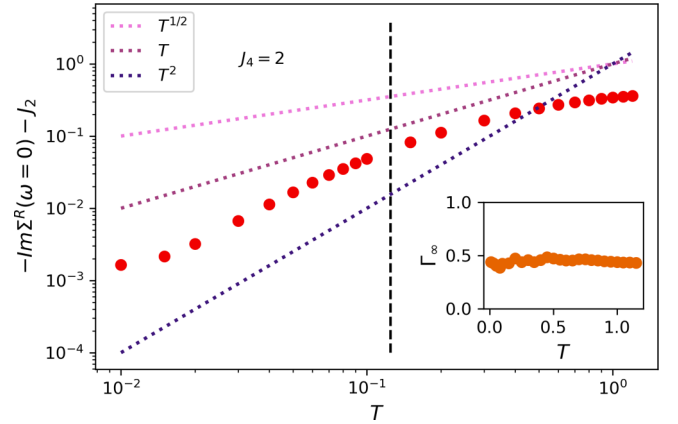

FIG. 12. Equilibrium scattering rate, defined as the imaginary part of the retarded self-energy in equilibrium at zero frequency, $-\mathrm{Im}\,\Sigma^R(\omega = 0)$, as a function of temperature. We see the crossover from FL ($-\mathrm{Im}\,\Sigma^R \sim T^2$) to NFL ($-\mathrm{Im}\,\Sigma^R \sim \sqrt{T}$) scaling, as the temperature is raised above T^* (dashed line), with an almost linear regime around the crossover. For comparison we plot in the inset the decay rate of the equilibrium retarded Green's function, equivalent to Γ_∞ defined in Sec. III, that show a featureless dependence from the temperature.

limit. In this case, the Dyson equation for the retarded single-particle Green's function can be written directly in frequency as

$$G^R(\omega) = \frac{1}{\omega - \Sigma^R(\omega)}, \qquad (A1)$$

where the retarded self-energy can be still written in the time domain as

$$\Sigma^R(t) = -\frac{J_4^2}{4}\left((G^R(t))^3 + 3G^R(t)G^K(t)^2\right) + J_2^2 G^R(t), \quad (A2)$$

where the Keldysh component $G^K(t)$ is related to the retarded one by the fluctuation-dissipation theorem, Eq. (18) of the main text. The two equations above can be solved iteratively, going back and forth from the frequency to the time domain, until a converged solution is found. A key feature of the equilibrium $SYK_4 + SYK_2$ model is the crossover from NFL to FL scaling as the temperature of the system is lowered below the scale $T^* \sim J_2^2/J_4$. This crossover can be clearly seen in the equilibrium scattering rate of the Majorana fermions, given by the imaginary part of the retarded self-energy at zero frequency that we plot in Fig. 12 as a function of temperature. We see that the low-temperature T^2 behavior crosses over to a square root scaling $\sim \sqrt{T}$, expected from SYK_4, when the temperature is above the dashed line, indicating the crossover scale T^* at that values of J_2, J_4, with an apparent linear regime around T^*. At higher temperatures, instead, the scattering rate saturates. We further note that in Fig. 12 the scattering rate is shifted with respect to a constant value proportional to J_2, the single-particle bandwidth, that is also responsible for a finite imaginary part of the self-energy from Eq. (A2), although not related to the many-body interactions. For comparison, we plot in the inset another measure of the decay rate, obtained from the long-time decay of the retarded Green's function, analogous to Γ_∞ defined in Sec. III. This quantity, on the other

hand, has a very weak dependence on temperature and does not show any signature of the crossover scale.

1. Effective temperature from energy conservation

We now discuss how to estimate the final effective temperature to which the system thermalizes after a given quench protocol from the knowledge of the equilibrium thermodynamics of the mixed SYK model. The total energy after the quench is, in fact, conserved and equal to

$$E_Q = \langle H_f \rangle_{H_i, T_i}, \tag{A3}$$

where $\langle \rangle_{H_i, T_i}$ indicates thermal averages over the initial Hamiltonian H_i at temperature T_i and H_f is the Hamiltonian driving the evolution after the quench. On the other hand, if the system thermalizes, one could expect the energy density to be given by the thermal expectation value of the final Hamiltonian at a temperature T_f, i.e.,

$$E_Q = E_T(T_f) = \langle H_f \rangle_{H_f, T_f}, \tag{A4}$$

where $\langle \rangle_{H_f, T_f}$ indicates thermal averages over the final Hamiltonian H_f at temperature T_f. Equation (A4) allows us to estimate the effective temperature from the knowledge of the energetics of the problem. The averages entering the equations above can be found by using functional derivatives and read

$$E_Q = i \frac{J_{2,i} J_{2,f}}{2} \int_0^\infty dt (G_i^>(t)^2 - G_i^<(t)^2), \tag{A5}$$

$$E_T(T_f) = i \frac{J_{2,f}^2}{2} \int_0^\infty dt (G_f^>(t)^2 - G_f^<(t)^2)$$
$$+ -i \frac{J_4^2}{2} \int_0^\infty dt (G_f^>(t)^4 - G_f^<(t)^4), \tag{A6}$$

where $G_i = G_{\text{SYK}_2, T=0}$ and $G_f = G_{\text{SYK}_4 + \text{SYK}_2, T_f}$. In Fig. 3, the solid line is the curve $T_f = T_f(J_4)$ obtained by this method.

APPENDIX B: QUANTUM BOLTZMANN EQUATION

In this Appendix, we sketch the derivation of the QBE for the mixed SYK model. We start from the real-time Dyson

Eq. (3) in the main text, that we write for the Keldysh component of the Green's function as

$$([G_0^R]^{-1} - \Sigma^R) \circ G^K = \Sigma^K \circ G^A, \tag{B1}$$

where $\circ$ is the real-time convolution and $[G_0^R]^{-1} = i\delta(t - t')\partial_t$ the noninteracting Majorana retarded Green's function. We then parametrize the Keldysh Green's function in terms of the distribution function $F(t_1, t_2)$ as $G^K = G^R \circ F - F \circ G^A$ and recast Eq. (B1) into a quantum kinetic equation form [35]

$$[\partial_{t_1}, F] = i\Sigma^K - i(\Sigma^R \circ F - F \circ \Sigma^A), \tag{B2}$$

where $[\partial_{t_1}, F](t_1, t_2) = (\partial_{t_1} + \partial_{t_2})F(t_1, t_2)$. To take the Wigner transform of this equation, we need to take care of the convolution. The Wigner transform of $f = g \circ h$ is [35]

$$f(\mathcal{T}, \omega) = g(\mathcal{T}, \omega) e^{-\frac{i}{2}(\overleftarrow{\partial_\mathcal{T}} \overrightarrow{\partial_\omega} - \overleftarrow{\partial_\omega} \overrightarrow{\partial_\mathcal{T}})} h(\mathcal{T}, \omega) \tag{B3}$$

$$= g(\mathcal{T}, \omega) h(\mathcal{T}, \omega) - \frac{i}{2} [\partial_\mathcal{T} g \partial_\omega h - \partial_\omega g \partial_\mathcal{T} h] + \cdots . \tag{B4}$$

We made a gradient expansion on the second line, valid for large central time $\mathcal{T}$. To lowest order in the gradient expansion, the kinetic equation reads

$$\partial_\mathcal{T} F(\mathcal{T}, \omega) = i\Sigma^K(\mathcal{T}, \omega)$$
$$- iF(\mathcal{T}, \omega)(\Sigma^R(\mathcal{T}, \omega) - \Sigma^A(\mathcal{T}, \omega)). \tag{B5}$$

After the quenc, the self-energies $\Sigma^K(t_1, t_2)$, $\Sigma^R(t_1, t_2) - \Sigma^A(t_1, t_2)$ are (where we omit the time-dependence for simplicity)

$$\Sigma^K = J_{2,f}^2 G^K - \frac{J_4^2}{4}[(G^K)^3 + 3G^K(G^R - G^A)^2] \tag{B6}$$

$$\Sigma^R - \Sigma^A = J_{2,f}^2 (G^R - G^A) - \frac{J_4^2}{4}[(G^R - G^A)^3$$
$$+ 3(G^R - G^A)(G^K)^2]. \tag{B7}$$

Taking the Wigner transform of these expressions and using the fact that $iG^K(\mathcal{T}, \omega) = A(\mathcal{T}, \omega)F(\mathcal{T}, \omega)$ and $G^R(\mathcal{T}, \omega) - G^A(\mathcal{T}, \omega) = 2i\text{Im}G^R(\mathcal{T}, \omega) = -iA(\mathcal{T}, \omega)$, we obtain for the two self-energies Σ^K, $\Sigma^R - \Sigma^A$ entering Eq. (B5) the results

$$\Sigma^K(\mathcal{T}, \omega) = J_{2,f}^2 G^K(\mathcal{T}, \omega) - i\frac{J_4^2}{4} \int \frac{d\omega_1}{2\pi} \frac{d\omega_2}{2\pi} A(\mathcal{T}, \omega - \omega_1 - \omega_2) A(\mathcal{T}, \omega_1) A(\mathcal{T}, \omega_2)$$
$$\times [F(\mathcal{T}, \omega - \omega_1 - \omega_2)F(\mathcal{T}, \omega_1)F(\mathcal{T}, \omega_2) + 3F(\mathcal{T}, \omega - \omega_1 - \omega_2)], \tag{B8}$$

$$\Sigma^R(\mathcal{T}, \omega) - \Sigma^A(\mathcal{T}, \omega) = -iJ_{2,f}^2 A(\mathcal{T}, \omega) - i\frac{J_4^2}{4} \int \frac{d\omega_1}{2\pi} \frac{d\omega_2}{2\pi} A(\mathcal{T}, \omega - \omega_1 - \omega_2) A(\mathcal{T}, \omega_1) A(\mathcal{T}, \omega_2)$$
$$\times [1 + 3F(\mathcal{T}, \omega_1)F(\mathcal{T}, \omega_2)].$$

Plugging these into Eq. (B5), we finally obtain a quantum kinetic equation for the distribution function, i.e.,

$$\partial_\mathcal{T} F(\mathcal{T}, \omega) = I^{\text{coll}}[F(\mathcal{T}, \omega)], \tag{B9}$$

where the collision integral I^{coll} can be rewritten after some simple manipulations as

$$I^{\text{coll}}[F(\mathcal{T}, \omega)] = \frac{J_4^2}{4} \int \frac{d\omega_1}{2\pi} \frac{d\omega_2}{2\pi} A(\mathcal{T}, \omega - \omega_1 - \omega_2) A(\mathcal{T}, \omega_1) A(\mathcal{T}, \omega_2) \times [F(\mathcal{T}, \omega - \omega_1 - \omega_2)F(\mathcal{T}, \omega_1)F(\mathcal{T}, \omega_2)$$
$$+ F(\mathcal{T}, \omega - \omega_1 - \omega_2) + F(\mathcal{T}, \omega_1) + F(\mathcal{T}, \omega_2) - F(\mathcal{T}, \omega)(1 + F(\mathcal{T}, \omega_1)F(\mathcal{T}, \omega_2)$$
$$+ F(\mathcal{T}, \omega - \omega_1 - \omega_2)F(\mathcal{T}, \omega_1) + F(\mathcal{T}, \omega - \omega_1 - \omega_2)F(\mathcal{T}, \omega_2))]. \tag{B10}$$

Interestingly. we note that the term in the self-energies proportional to $J_{2,f}^2$ in Eqs. (B8) drops out of the expression for the collision integral $I^{\text{coll}}[F]$, at least to the lowest order. This underlies the fact that the J_2 coupling, while resulting in a self-energy contribution for the Majorana mode after disorder averaging, does not provide an effective scattering mechanism. This is further indication that the pure SYK$_2$ is not able to reach thermal equilibrium by itself. We also note that the collision integral in Eq. (B10) has a specific dependence from the distribution function $F(\mathcal{T}, \omega)$. In fact, one can show, using the properties of the hyperbolic tangent function, that for an equilibrium distribution function the collision integral vanishes exactly, i.e.,

$$I^{\text{coll}}[F^{\text{eq}}(\omega)] = 0 \quad \text{where} \quad F^{\text{eq}}(\omega) = \text{th}\left(\frac{\beta\omega}{2}\right), \quad \text{(B11)}$$

properties which guarantees that the QBE dynamics leads to thermal equilibrium. We note, however, that the temperature β in the above equation is only fixed by the initial condition. As for the distribution function, we can also write an equation for the spectral density $A(\mathcal{T}, \omega)$. We start from the left and right Dyson equations for the retarded component of the Green's function:

$$G_0^{-1} \circ G^R = 1 + \Sigma^R \circ G^R, \quad \text{(B12)}$$

$$G^R \circ G_0^{-1} = 1 + G^R \circ \Sigma^R. \quad \text{(B13)}$$

We subtract the two equations:

$$\left[G_0^{-1} - \Sigma^R, G^R \right] = 0; \quad \text{(B14)}$$

likewise for the advanced component:

$$\left[G_0^{-1} - \Sigma^A, G^A \right] = 0. \quad \text{(B15)}$$

We can rewrite these two equations in terms of $G_\pm = (G^R \pm G^A)/2$ and $\Sigma_\pm = (\Sigma^R \pm \Sigma^A)/2$:

$$\left[G_0^{-1} - (\Sigma_+ + \Sigma_-), G_+ + G_- \right] = 0, \quad \text{(B16)}$$

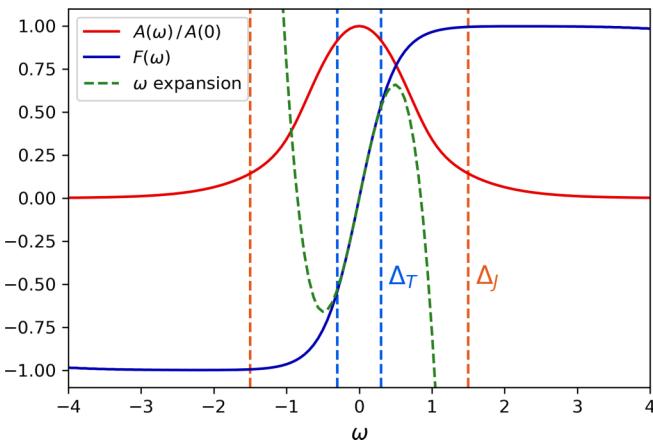$$\left[G_0^{-1} - (\Sigma_+ - \Sigma_-), G_+ - G_- \right] = 0. \quad \text{(B17)}$$

FIG. 13. Frequency dependence of spectral and distribution functions at long times $\mathcal{T} = \mathcal{T}_{\max}$ for the mixed SYK model after a quench to $J_2 = 0.5$, $J_4 = 1.5$, leading to a final temperature $T_f \simeq 0.25$.

The difference of these two equations is

$$\left[G_0^{-1}, G_- \right] = [\Sigma_+, G_-] + [\Sigma_-, G_+]. \quad \text{(B18)}$$

We now take the Wigner transform of this equation and keep only the lowest order terms in the gradient expansion. According to Eq. (B3), the Wigner transform of a commutator (for the convolution) is zero at lowest order, so the right-hand side yields zero. As $G_-(\mathcal{T}, \omega) = -iA(\mathcal{T}, \omega)/2$, we have

$$\partial_{\mathcal{T}} A(\mathcal{T}, \omega) = 0. \quad \text{(B19)}$$

This is consistent with the results obtained by numerically solving the KM equation. The gradient expansion is valid only for large central time $\mathcal{T}$ and we have in the numerics that the spectral function $A(\mathcal{T}, \omega)$ equilibriates shortly after the quench while the distribution function $F(\mathcal{T}, \omega)$ takes a longer time.

1. Approximate Solution of QBE for the mixed SYK model

In the main text, we have presented the full QBE numerical solution starting from an initial condition obtained through a short-time propagation of KB equations. This hybrid approach, which we have shown to compare well with the exact KB dynamics for the mixed SYK model, could be particularly useful to study systems with slow dynamics, which can be challenging to tackle with a full KB simulation on very long timescales. Still, the computational effort associated with a QBE simulation remains substantial due to the frequency convolution structure of the collision integral in Eq. (B10). A possible approach, developed in Ref. [39] to study quenches of interacting bosonic field theories, is to focus on the low-frequency part of the distribution function and to parametrize it in terms of few time-dependent coefficients within a small ω expansion

$$F(\mathcal{T}, \omega) = \frac{\beta(\mathcal{T})}{2}\omega + C(\mathcal{T})\omega^3 + \cdots, \quad \text{(B20)}$$

leading to a set of simple rate equations for the effective temperature and other time-dependent parameters, whose numerical integration could be performed very efficiently. In Ref. [39], this approach was shown to capture qualitatively well the QBE dynamics. In the case of the mixed SYK model, however, we found this simple approximation to break down. This is due to the fact that a low-frequency expansion for the distribution function only holds if

$$\omega \ll \Delta_T \sim \min(T_i, T_f). \quad \text{(B21)}$$

At the same time, the structure of the collision integral is such that the distribution function always appears multiplied by the spectral function A at the same frequency. Thus, it is a good approximation to expand F in powers of ω if the bandwidth Δ_J of A is smaller or of the order of Δ_T. This is typically the case when sharp quasiparticle excitations dominate the spectrum. On the other hand, for SYK models we typically have very broad spectral functions with bandwidth $\Delta_J \sim J \gg \Delta_T$. This is shown for concreteness in Fig. 13, where we compare spectral and distribution functions a long time after a quench to $J_2 = 0.5$, $J_4 = 1.5$, leading to a final

temperature $T_f \simeq 0.25$. This further confirms that quasiparticlelike approximations to the QBE are likely not able to capture the dynamics of SYK models and one needs to resort to the full solution of the QBE.

[1] S. Sachdev and J. Ye, Gapless Spin-Fluid Ground State in a Random Quantum Heisenberg Magnet, Phys. Rev. Lett. **70**, 3339 (1993).

[2] A. Kitaev, A simple model of quantum holography, KITP strings seminar and Entanglement 2015 program (unpublished).

[3] A. Kitaev and S. J. Suh, The soft mode in the Sachdev-Ye-Kitaev model and its gravity dual, J. High Energy Phys. 05 (2018) 183.

[4] J. Maldacena and D. Stanford, Remarks on the Sachdev-Ye-Kitaev model, Phys. Rev. D **94**, 106002 (2016).

[5] J. Polchinski and V. Rosenhaus, The spectrum in the Sachdev-Ye-Kitaev model, J. High Energy Phys. 04 (2016) 1.

[6] D. Bagrets, A. Altland, and A. Kamenev, Sachdev-Ye-Kitaev model as Liouville quantum mechanics, Nucl. Phys. B **911**, 191 (2016).

[7] D. Bagrets, A. Altland, and A. Kamenev, Power-law out of time order correlation functions in the SYK model, Nucl. Phys. B **921**, 727 (2017).

[8] S. Sachdev, Bekenstein-Hawking Entropy and Strange Metals, Phys. Rev. X **5**, 041025 (2015).

[9] D. Chowdhury, A. Georges, O. Parcollet, and S. Sachdev, Sachdev-Ye-Kitaev models and beyond: A window into non-Fermi liquids, arXiv:2109.05037.

[10] A. V. Lunkin, K. S. Tikhonov, and M. V. Feigel'man, Sachdev-Ye-Kitaev Model with Quadratic Perturbations: The Route to a Non-Fermi Liquid, Phys. Rev. Lett. **121**, 236601 (2018).

[11] A. Altland, D. Bagrets, and A. Kamenev, Quantum Criticality of Granular Sachdev-Ye-Kitaev Matter, Phys. Rev. Lett. **123**, 106601 (2019).

[12] A. V. Lunkin, A. Y. Kitaev, and M. V. Feigel'man, Perturbed Sachdev-Ye-Kitaev Model: A Polaron in the Hyperbolic Plane, Phys. Rev. Lett. **125**, 196602 (2020).

[13] O. Parcollet and A. Georges, Non-Fermi-liquid regime of a doped Mott insulator, Phys. Rev. B **59**, 5341 (1999).

[14] A. Georges, O. Parcollet, and S. Sachdev, Quantum fluctuations of a nearly critical Heisenberg spin glass, Phys. Rev. B **63**, 134406 (2001).

[15] P. Cha, N. Wentzell, O. Parcollet, A. Georges, and E.-A. Kim, Linear resistivity and Sachdev-Ye-Kitaev (SYK) spin liquid behavior in a quantum critical metal with spin-1/2 fermions, Proc. Natl. Acad. Sci. USA **117**, 18341 (2020).

[16] P. T. Dumitrescu, N. Wentzell, A. Georges, and O. Parcollet, Planckian metal at a doping-induced quantum critical point, arXiv:2103.08607.

[17] A. A. Husain, M. Mitrano, M. S. Rak, S. I. Rubeck, H. Yang, C. Sow, Y. Maeno, P. E. Batson, and P. Abbamonte, Coexisting Fermi liquid and strange metal phenomena in Sr$_2$RuO$_4$, arXiv:2007.06670.

[18] A. M. García-García, B. Loureiro, A. Romero-Bermúdez, and M. Tezuka, Chaotic-Integrable Transition in the Sachdev-Ye-Kitaev Model, Phys. Rev. Lett. **120**, 241603 (2018).

[19] M. Haque and P. A. McClarty, Eigenstate thermalization scaling in Majorana clusters: From chaotic to integrable Sachdev-Ye-Kitaev models, Phys. Rev. B **100**, 115122 (2019).

[20] T. Micklitz, F. Monteiro, and A. Altland, Nonergodic Extended States in the Sachdev-Ye-Kitaev Model, Phys. Rev. Lett. **123**, 125701 (2019).

[21] F. Monteiro, T. Micklitz, M. Tezuka, and A. Altland, Minimal model of many-body localization, Phys. Rev. Research **3**, 013023 (2021).

[22] X.-Y. Song, C.-M. Jian, and L. Balents, Strongly Correlated Metal Built from Sachdev-Ye-Kitaev Models, Phys. Rev. Lett. **119**, 216601 (2017).

[23] H. Guo, Y. Gu, and S. Sachdev, Transport and chaos in lattice Sachdev-Ye-Kitaev models, Phys. Rev. B **100**, 045140 (2019).

[24] J. Kim, X. Cao, and E. Altman, Scrambling versus relaxation in Fermi and non-Fermi liquids, Phys. Rev. B **102**, 085134 (2020).

[25] S. Banerjee and E. Altman, Solvable model for a dynamical quantum phase transition from fast to slow scrambling, Phys. Rev. B **95**, 134302 (2017).

[26] J. Kim and X. Cao, Comment on "Chaotic-Integrable Transition in the Sachdev-Ye-Kitaev Model", Phys. Rev. Lett. **126**, 109101 (2021).

[27] A. M. García-García, B. Loureiro, A. Romero-Bermúdez, and M. Tezuka, García-García *et al.* Reply:, Phys. Rev. Lett. **126**, 109102 (2021).

[28] A. Eberlein, V. Kasper, S. Sachdev, and J. Steinberg, Quantum quench of the Sachdev-Ye-Kitaev model, Phys. Rev. B **96**, 205123 (2017).

[29] R. Bhattacharya, D. P. Jatkar, and N. Sorokhaibam, Quantum quenches and thermalization in SYK models, J. High Energy Phys. 07 (2019) 066.

[30] T. Samui and N. Sorokhaibam, Thermalization in different phases of charged SYK model, J. High Energy Phys. 04 (2021) 157.

[31] A. Haldar, P. Haldar, S. Bera, I. Mandal, and S. Banerjee, Quench, thermalization, and residual entropy across a non-Fermi liquid to Fermi liquid transition, Phys. Rev. Research **2**, 013307 (2020).

[32] I. Kourkoulou and J. Maldacena, Pure states in the SYK model and nearly-*AdS*$_2$ gravity, arXiv:1707.02325.

[33] P. Zhang, Entanglement entropy and its quench dynamics for pure states of the Sachdev-Ye-Kitaev model, J. High Energy Phys. 06 (2020) 143.

[34] C. Kuhlenkamp and M. Knap, Periodically Driven Sachdev-Ye-Kitaev Models, Phys. Rev. Lett. **124**, 106401 (2020).

[35] A. Kamenev, *Field Theory of Non-Equilibrium Systems* (Cambridge University Press, Cambridge, United Kingdom, 2011).

[36] L. Kadanoff and G. Baym, *Quantum Statistical Mechanics* (CRC Press, Boca Raton, Florida, 1962).

[37] A. Altland and B. D. Simons, *Condensed Matter Field Theory*, 2nd ed. (Cambridge University Press, Cambridge, United Kingdom, 2010).

[38] M. Lindner and M. M. Müller, Comparison of Boltzmann equations with quantum dynamics for scalar fields, Phys. Rev. D **73**, 125002 (2006).

[39] M. Tavora and A. Mitra, Quench dynamics of one-dimensional bosons in a commensurate periodic potential: A quantum kinetic equation approach, Phys. Rev. B **88**, 115144 (2013).

[40] A. Picano, J. Li, and M. Eckstein, Quantum Boltzmann equation for strongly correlated electrons, Phys. Rev. B **104**, 085108 (2021).

[41] J. Berges, S. Borsányi, and C. Wetterich, Prethermalization, Phys. Rev. Lett. **93**, 142002 (2004).

[42] M. Moeckel and S. Kehrein, Interaction Quench in the Hubbard Model, Phys. Rev. Lett. **100**, 175702 (2008).

[43] T. Langen, T. Gasenzer, and J. Schmiedmayer, Prethermalization and universal dynamics in near-integrable quantum systems, J. Stat. Mech. (2016) 064009.

[44] M. Schiró and A. Mitra, Transient Orthogonality Catastrophe in a Time-Dependent Nonequilibrium Environment, Phys. Rev. Lett. **112**, 246401 (2014).

[45] A. Mitra and T. Giamarchi, Mode-Coupling-Induced Dissipative and Thermal Effects at Long Times After a Quantum Quench, Phys. Rev. Lett. **107**, 150602 (2011).

[46] A. Mitra, Quantum quench dynamics, Annu. Rev. Condens. Matter Phys. **9**, 245 (2018).

[47] G. Folena, S. Franz, and F. Ricci-Tersenghi, Rethinking Mean-Field Glassy Dynamics and Its Relation with the Energy Landscape: The Surprising Case of the Spherical Mixed *p*-Spin Model, Phys. Rev. X **10**, 031045 (2020).